Phase-sensitive FMCW radar system for high-precision Antarctic ice shelf profile monitoring

Paul V. Brennan[1], Lai Bun Lok[1], Keith Nicholls[2], Hugh Corr[2]

[1]*Department of Electronic & Electrical Engineering, University College London, Torrington Place, London WC1E 7JE, UK*
[2]*British Antarctic Survey, High Cross, Madingley Road, Cambridge CB3 0ET, UK*
E-mail: p.brennan@ucl.ac.uk

Abstract: Ice shelves fringe much of the Antarctic continent, and, despite being up to 2 km thick, are vulnerable to climate change. Owing to their role in helping to control the ice sheet contribution to sea level change there is great interest in measuring the rate at which they are melting into the ocean. This study describes the development and deployment of an ice-penetrating phase-sensitive FMCW radar, sufficiently robust and with sufficiently low-power consumption to be run through the Antarctic winter as a standalone instrument, yet with the stability and mm-precision needed to detect the very slow changes in ice shelf thickness in this exceptionally demanding environment. A number of elegant processing techniques are described to achieve reliable, high-precision performance and results presented on field data obtained from the Larsen-C ice shelf, Antarctica.

1 Introduction

Concern is growing that the ability to predict future sea level rise is being compromised by the inability to predict the discharge of ice from the Antarctic ice sheet into the ocean. Ice shelves, the floating extension of the ice sheet, fringe the majority of Antarctica, and their presence impedes drainage of continental ice. The fate of ice shelves in a warming climate is therefore of great, and growing, interest. The key to determining the future of ice shelves is to observe how the rate of melting at their base responds to seasonal and inter-annual variations in the oceanographic forcing. The British Antarctic Survey pioneered the use of phase-sensitive, ground-based, ice-penetrating radar (pRES) in order to measure basal melt rates to precisions of mm/year [1]. The system relies on being able to detect the ice base, and also the relatively weak internal reflecting layers that are caused by changes in ice permittivity. The pRES instrument consists of an HP8751A network analyser configured as a step-frequency radar, utilising a pair of 10 dBi UHF antennas, of 5 m separation, operated at a centre frequency of 305 MHz, with a bandwidth of 160 MHz and a frequency step size of 32 kHz.

The pRES system has successfully measured ice shelf depths [1, 2], including basal layer and internal layers, in a number of locations over the George VI Ice Shelf and Ronne Ice Shelf, Antarctica. The pRES instrument has since been applied to ground-based ice sheets, to track internal layers to learn more about the dynamics of ice flow. This system, however, suffers from a number of limitations. Being based on a general-purpose network analyser, the receiver noise figure is high – of the order of 30 dB. As a result, very long measurement times, of typically 100–1000 s, are required to obtain sufficient signal-to-noise ratio (SNR). However, since the target scene is very slow moving such long measurement times are entirely feasible. A further difficulty with pRES is that the power consumption of the network analyser is high and a petrol-generator is required in order to operate the instrument. It is also bulky and not able to operate to particularly low temperature. The net effect of these limitations is that it is not practical to operate the instrument autonomously over a long time period, such as a complete year or beyond, thus restricting data sets to a series of snapshots only during Austral summers.

In view of the enormous potential of pRES, a purpose-built radar system (the subject of this paper) is under development, specifically optimised for this application. Although this system has similar range resolution performance to pRES, it has far lower noise figure and power consumption, allowing the possibility of year-round operation from a modest set of batteries and solar panel. The system, outlined in Fig. 1, comprises a phase-sensitive FMCW radar based on a direct digital synthesiser (DDS) linear-FM chirp generator, a low-noise receiver/downconvertor chain and, crucially, a means of synchronising the baseband, deramped signal to allow precise phase measurement in subsequent processing in order to enhance the range precision to well beyond that of the standard range resolution. Cardenas *et al.* [3] have recently used FMCW radar for a similar purpose, but without phase processing and with far reduced resolution, of the order of 1 m. Other researchers [4, 5] have used satellite radar altimetry to image Antarctic ice shelf thickness and sea ice, which has the benefit of mapping a very large area, but with modest depth precision, of around 20 cm. In addition, the pulsed nature of these altimeters is
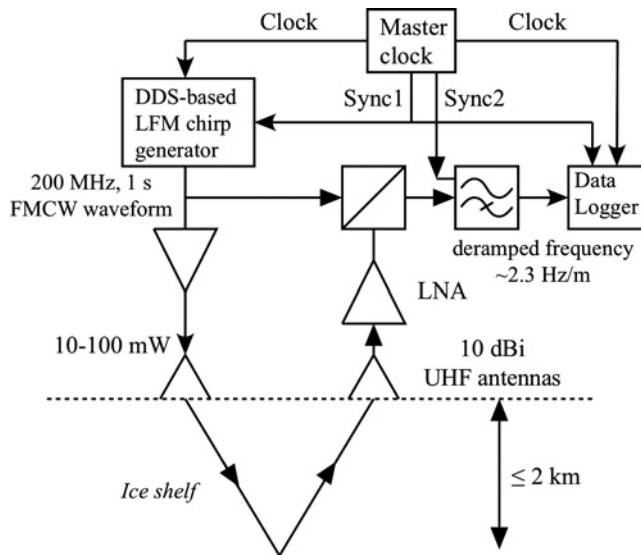
Fig. 1 *Simplified block diagram of the basic phase-sensitive FMCW radar instrument*

less suited to this application in view of the need for very high-precision through a lossy medium with low DC power requirements, which would favour the use of pulse compression. The power consumption of our system is of the order of 5 W during operation and 1 mW during standby. The much reduced noise figure relative to pRES enables signal collection in around 1 s, although in practice an operating time of around 1 min is likely to allow for a variety of receive gain combinations and the prospect of pulse-to-pulse averaging if necessary. The on/standby duty cycle is around 1 min per 6 h, and hence the mean power consumption is ~31 mW, allowing operation over a complete winter from a modest accumulator of some 40 Ah capacity. The system is designed with components specified to −40°C. Communication may be via an Iridium satellite link or by manual data retrieval during the Antarctic summer.

2   System considerations and link budget

The baseband or deramped frequency of an FMCW radar, f_d, and the range resolution, ΔR, are given by the well-known expressions [6]

$$f_d = \frac{2BR\sqrt{\varepsilon_r}}{Tc} \quad \Delta R = \frac{c}{2B\sqrt{\varepsilon_r}} \quad (1)$$

where B is the sweep bandwidth, R is the range to a target, T is the pulse duration, c is the speed of light and ε_r is the dielectric constant of the medium which, for ice, is typically 3.1. In a dispersive medium, the range resolution is degraded slightly, which can be represented by an empirical factor in (1) (e.g. 1.39 as proposed in [7]). The new radar system is designed for a similar operating frequency and bandwidth to pRES, with a centre frequency of 300 MHz and a sweep bandwidth, B, of 200 MHz, giving a deramped frequency of some 2.35 Hz/m, assuming 1 s pulse duration, and a range resolution of 43 cm. Millimetre range precision is achieved by means of careful phase measurement of the deramped pulses. The deramped frequency at maximum range (2 km) is some 4.7 kHz, requiring a modest data logger sampling rate of around 12 ksamples/s or greater.

The radar is required to detect echoes from the ice shelf base, which typically has a high-reflection coefficient of some −2 dB, and internal layers that are closer but have rather lower-reflection coefficients, in the range −60 to −90 dB. Knowledge of the variation of echo power with depth is important in order to determine radar design parameters, such as pulse duration/integration time, receive path gain and appropriate design of the baseband high-pass filter to best compensate for the range-dependent signal level.

The echo power variation depends on the nature of the reflecting interface. It is known that the basal layer of an ice shelf is highly irregular, with a surface roughness that is large relative to the radar wavelength suggesting Bragg scattering [8], in which case the surface can be assumed to scatter energy equally in all directions, as depicted in Fig. 2. FMCW radar operation will act to combine the powers of echoes occurring over ranges differing by the range resolution, ΔR. From Fig. 2, assuming that the system is resolution-limited with an antenna beamwidth exceeding the resolution-limited footprint, a circular region is illuminated on the scattering layer responsible for scattering the power appearing in a given range bin, at range R, with the following radius

$$r = \sqrt{2R\Delta R} \quad (2)$$

The range estimate obtained by the radar is actually a result of the mean distance to a given layer of the ice, averaged over the circular range resolution footprint of radius r. The angle subtended by the resolution-limited footprint on a layer of depth R is given by

$$\alpha \simeq \frac{2r}{R} = \sqrt{\frac{8\Delta R}{R}} \quad (3)$$

indicating that for a depth of 100 m (a likely lower bound) the antenna beamwidth needs to be at least 10.6° for the system to be resolution-limited. In this system, the antennas have a modest gain of around 10 dBi with beamwidths of around 60° and so the system is very much resolution-limited. The power intercepted by this region of the target is given by the product of its area and the power density of the signal transmitted from the radar

$$P_{int} = \frac{P_t G}{4\pi R^2} \pi r^2 = \frac{P_t G}{4\pi R^2} 2\pi R\Delta R = \frac{P_t G\Delta R}{2R} \quad (4)$$
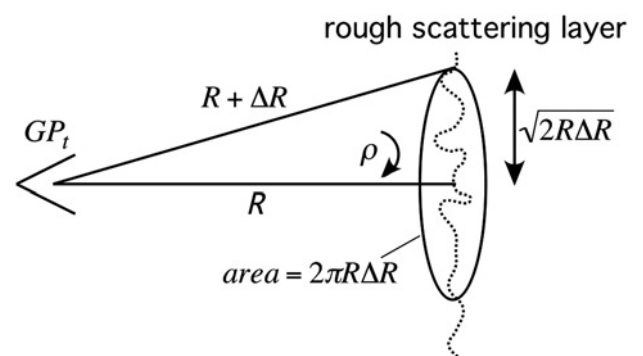
Fig. 2 *Construction to calculate scattering from a rough layer*
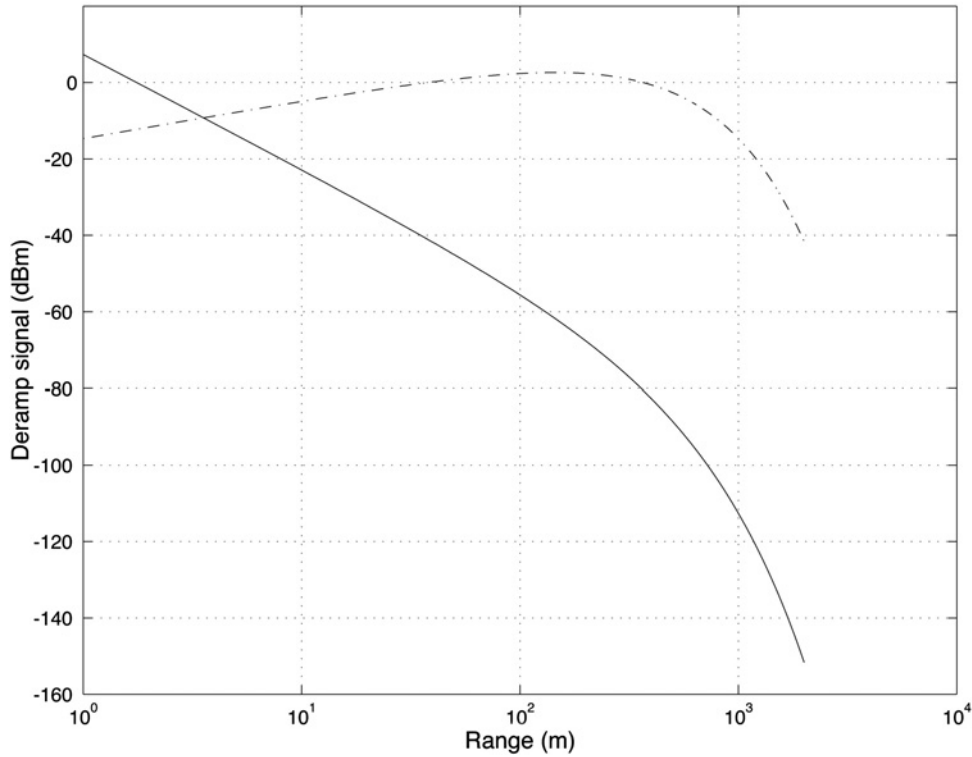
Fig. 3 *Predicted echo power level, at radar input (solid) and high-pass filtered baseband output (dashed), assuming 0.015 dB/m ice attenuation*

Assuming this power is scattered evenly over a hemisphere in the direction of the transmit source, the echo power collected at the receiver is

$$P_r = \frac{P_t G \Delta R \rho L}{2R} \frac{G\lambda^2/4\pi}{2\pi R^2} = \frac{P_t G^2 \rho L \lambda^2 \Delta R}{16\pi^2 R^3} \qquad (5)$$

where R is the distance to the target layer, P_t is the transmit RF power, G is the transmit/receive antenna gain, λ is the wavelength in ice and L is the loss (≤ 1) of the ice medium (typically 0.01–0.02 dB/m in glacier ice at frequencies below 600 MHz), demonstrating an inverse-cube law relation with range. Fig. 3 shows the predicted variation of echo power with distance [(5)], assuming 43 cm range resolution, a reflection coefficient, ρ, of −2 dB (typical of the ice base), and an attenuation coefficient of 0.015 dB/m. The echo power falls with range initially at a rate of 30 dB/decade, until around 100 m range, and then more rapidly. This characteristic may be compensated by a second-order high-pass filter in the baseband path, as is common practice in FMCW radar, also shown in Fig. 3. The high-pass filter has a fixed slope of +40 dB/decade, which over-compensates the signal level variation at shorter ranges, but under-compensates at longer ranges. This would therefore seem to be a good compromise, reducing the dynamic range of the signal applied to the ADC in the data logger from some 120 to 40 dB, over a projected operating range of 10–1600 m, suggesting that an ADC with 60 dB dynamic range or greater, equivalent to an effective number of bits (ENOBs) of 10 should be sufficient. In practice, at such very low sampling rates (40 ksamples/s), ADCs with 16–20 ENOBs are readily available.

The SNR of the received echo may readily be obtained from (5) by including the thermal noise term associated with a receiver bandwidth of $1/T$ and noise factor, F

$$\mathrm{SNR} = \frac{P_r T}{kT_a F} = \frac{P_t G^2 \rho L \lambda^2 \Delta R T}{16\pi^2 kT_a F R^3} \qquad (6)$$

The phase of the returned echo is used to derive a high-precision range estimate of any point target and so the phase noise corresponding to the above SNR is of importance. For a relatively small phase noise (<15° RMS), the relationship between additive SNR and associated phase noise is given by the following analytic expression [9, 10]

$$\Delta\phi_{\mathrm{rms}} = \frac{1}{\sqrt{2\ \mathrm{SNR}}} \qquad (7)$$

yielding a simple result for the RMS range measurement error

$$R_{\mathrm{error}}(\mathrm{rms}) = \frac{\lambda}{4\pi}\Delta\phi_{\mathrm{rms}} = \frac{\lambda}{4\pi\sqrt{2\ \mathrm{SNR}}} \qquad (8)$$

this expression being valid for SNR values of around 10 dB or above. The results of the latter two expressions are shown in Figs. 4 and 5, again for the radar parameters of this system, including a pulse duration, T, of 1 s and a noise figure of 6 dB. From Fig. 4, the expected SNR is clearly excellent (>75 dB) for an ice base closer than 500 m, but then falls rapidly as a result of both the inverse-cube dependence and the ice attenuation. At 2 km, the expected SNR is around 14 dB. The corresponding range measurement error, Fig. 5, is below 1 mm RMS for ranges up to 1500 m, and then degrades to some 3 mm RMS at 1800 m and 7 mm RMS at 2000 m. The maximum range at which the instrument is likely to be used in planned trials is
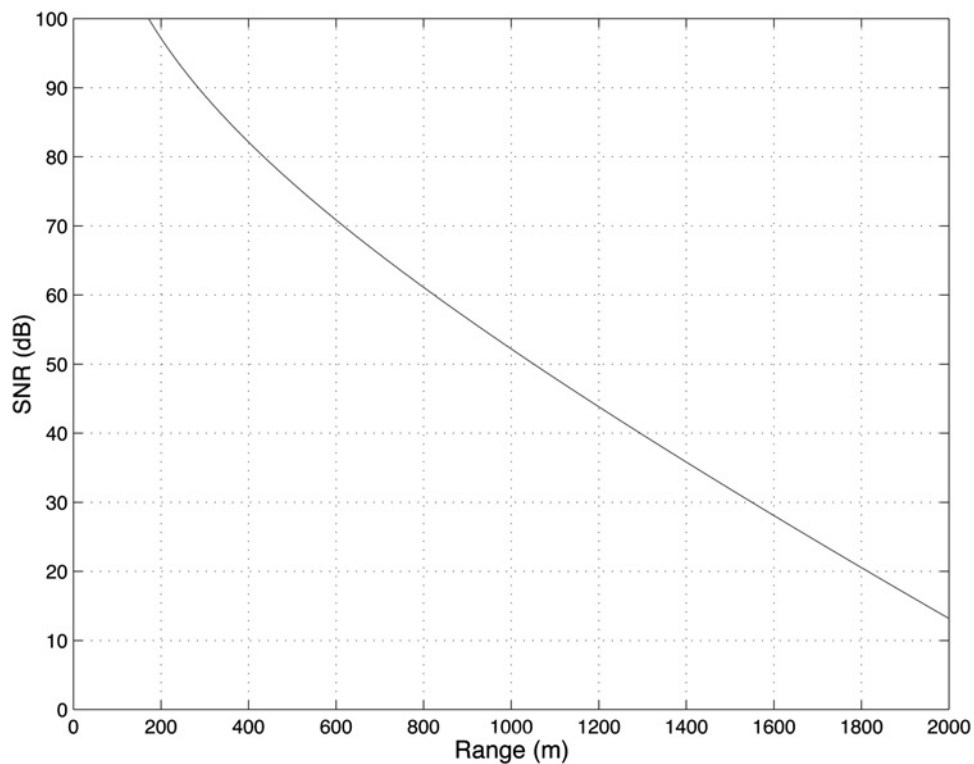
Fig. 4 *Predicted SNR, assuming 1 s pulse duration, 6 dB receiver noise figure and 0.015 dB/m ice attenuation*
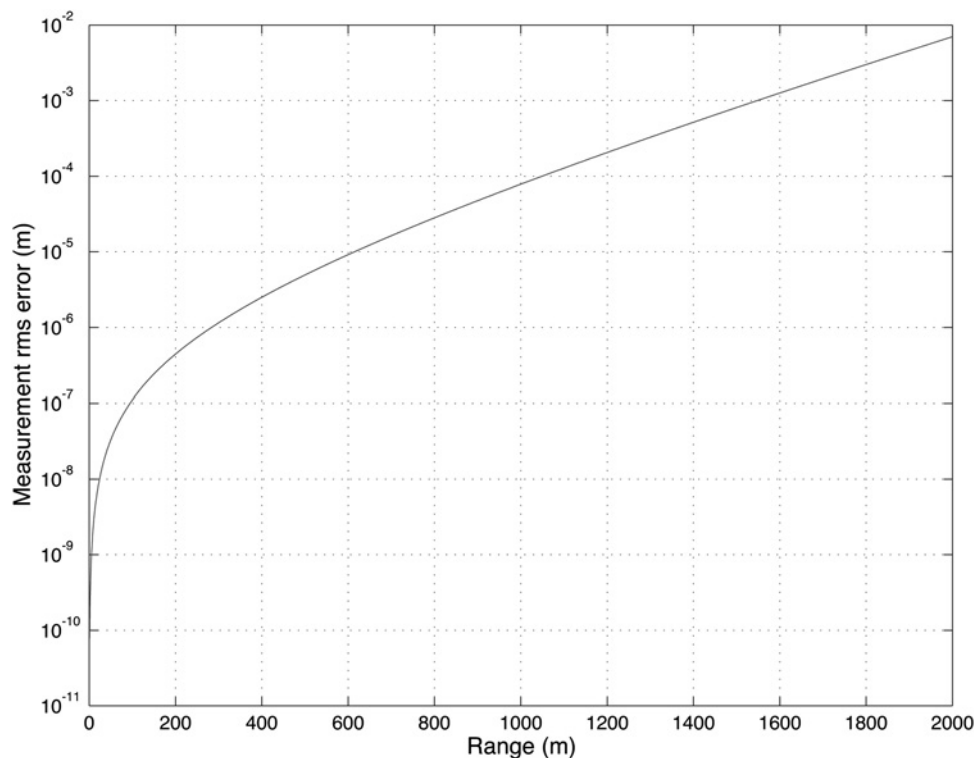
Fig. 5 *Predicted RMS range error because of noise, assuming 1 s pulse duration, 6 dB receiver noise figure and 0.015 dB/m ice attenuation*

1800 m. Coherent pulse averaging may be employed, if required, to reduce the range measurement error – averaging ten pulses yielding a predicted 1 mm RMS error at 1800 m range. The principal radar parameters and values assumed for the prototype system are summarised in Table 1.

3 Phase-sensitive FMCW radar signal processing

This instrument presents some interesting data processing and hardware synchronisation challenges, some of which are

Table 1 Principal radar parameters

Operating frequency (centre), f_c	300 MHz
FM sweep bandwidth, B	200 MHz
RF power, P_t	20 dBm
Antenna gains, G_t, G_r	10 dBi
Noise figure, N	6 dB ($F = 4$)
Associated standard range resolution, ΔR	43 cm with $\varepsilon_r = 3.1$
Depth precision in phase-sensitive mode	3 mm RMS, provided SNR >21 dB
Pulse duration, T	1 s
Total acquisition time	60 s for c. Ten pulses each with four RF gain values
ADC sampling rate	>12 ksamples/s
Ice attenuation	0.015 dB/m
Maximum operating range, R	2 km
Reflection coefficient between internal layers, ρ	−60 to −90 dB
Reflection coefficient at ice sheet base, ρ	−2 dB

addressed in previous work [11–13] on high-precision ranging. Ayhan *et al.* [11] present an interesting technique to improve the frequency precision estimate in an FMCW radar and hence to improve the range precision; however, it has difficulties at lower frequencies because of spectrum fold-over and is slightly more vulnerable to noise. The processing presented here represents a clear and comprehensive technique to unambiguously achieve high-precision range profiling in phase-sensitive FMCW radar at both long and short ranges. To understand the required processing steps, an analysis of linear-FMCW radar is necessary, as follows.

The radar transmit signal instantaneous frequency may be described by

$$\omega_t(t) = \omega_c + K(t - T/2), \quad 0 \le t \le T \quad (9)$$

where ω_c is the centre frequency, T is the pulse duration and K is the FM sweep rate (rad/s^2). Integrating, the corresponding transmit signal instantaneous phase is given by

$$\phi_t(t) = \omega_c t + \frac{Kt^2}{2} - \frac{KTt}{2} + \text{const}, \quad 0 \le t \le T \quad (10)$$

where the FM sweep rate, K, is related to the FM sweep bandwidth, B, and pulse duration, T, as follows

$$K = 2\pi B/T \quad (11)$$

The received echo from a point target at range R arrives at the radar with phase

$$\phi_r(t) = \omega_c(t - \tau) + \frac{K(t - \tau)^2}{2} - \frac{KT(t - \tau)}{2} + \text{const} \quad (12)$$

where $\tau = 2R\sqrt{\varepsilon_r}/c$ is the round-trip delay from the radar transmitter to receiver. Finally, the deramped signal phase is the difference between the transmit and receive signal phases

$$\phi_d(t) = \phi_t - \phi_r = \omega_c \tau + K\tau(t - T/2) - K\tau^2/2 \quad (13)$$

where $\omega_c \tau$ is the crucial phase term that is used in this instrument to provide high-precision range estimation to distinct targets, $K\tau(t - T/2)$ is a time-linear phase term

representing the frequency of the signal and $-K\tau^2/2$ is a (usually small) phase offset. Differentiating gives the well-known expression for the deramped frequency

$$\omega_d = K\tau = \frac{4\pi BR\sqrt{\varepsilon_r}}{cT} \text{ or}$$
$$f_d = \frac{2BR\sqrt{\varepsilon_r}}{cT} \quad (14)$$

FFT processing of the deramped pulse, of duration T, results in a range profile comprising range bins separated by $1/T$ in frequency and by the range resolution, ΔR [(1)] in range. For phase-sensitive operation, a Vernier-like process is used to combine standard FFT-based range processing, giving a coarse range estimate to the nearest range bin, $n\Delta R$ (in the absence of zero-padding), with a fine range estimate derived from the phase, $\omega_c \tau$, of the component within this range bin, where the fine range component is related to the measured phase, ϕ_d, by

$$R_{\text{fine}} = \frac{\lambda \phi_d}{4\pi} \quad (15)$$

where λ is the wavelength in the medium. This yields a range measurement precision, to a given distinct point target, which far exceeds that available from standard range processing alone. This process requires accurate measurement of the phase of the target return in a range bin close to that in which a distinct target is located. There are some practical issues. The phase variation of the deramped pulse from a target as it moves across a complete range bin of width $\Delta R = c/(2B\sqrt{\varepsilon_r})$, may be readily calculated

$$\begin{aligned} &\text{phase variation } \Delta(\omega_c \tau) \\ &= \omega_c(2\Delta R\sqrt{\varepsilon_r}/c) = \omega_c/B = 2\pi f_c/B \end{aligned} \quad (16)$$

Clearly, this phase variation should be no more than 2π rads to allow absolute unambiguous range measurement. Equation (16) thus indicates that at least 100% fractional bandwidth is necessary, requiring a truly ultra-wideband radar. This issue may be easily resolved by zero-padding the deramped echo prior to FFT processing, lengthening the time-sample by a 'pad factor', p, and thus reducing the spacing between range bins by the same factor, to $\Delta R/p$. For the present system, a pad factor of two is sufficient to reduce the intra-range bin phase change from 3π to 1.5π rads. Care is required to perform this zero-padding correctly. Equation (13) reveals that the phase centre of the deramped waveform is in the centre of the sample, at $t = T/2$; however, the phase indicated by an FFT is that at the start of the sample, at $t = 0$. It is therefore necessary to rotate the deramped (time-domain) waveform so that the centre of the waveform aligns with the start of the sample, $t = 0$, prior to FFT processing.

For processing convenience, it would be highly desirable if the phase relating to a point target located at the centre of each range bin is normalised to zero. This can be achieved by weighting the FFT-processed deramped waveform by a reference array equal to the phase conjugate of the expected phase at the centre of each range bin. From (13), such a

reference array is described by

$$\text{ref} = \exp\left(-j(\omega_c\tau - K\tau^2/2)\right)$$
$$= \exp\left(-j(n\omega_c/Bp - n^2K/2B^2p^2)\right) \tag{17}$$

which is expressed in the second line of (17) in a form that is suitable for the processing algorithm, in terms of the nth range bin, where the round-trip delay, τ_n, to targets centred in the nth range bin is given by

$$\tau_n = \frac{2\sqrt{\varepsilon_r}}{c}n\Delta R$$
$$= \frac{2\sqrt{\varepsilon_r}}{c}\frac{nc}{2B\sqrt{\varepsilon_r}p} = n/Bp \tag{18}$$

The chirp waveform and ADC need to be precisely synchronised to make an accurate phase measurement of the deramped echo; this can be achieved in practice by initiating the chirp with a frequency-divided version of the ADC sampling signal. If, however, there is a time delay, Δt, because of mis-synchronisation, then this will result in a phase error, $\Delta\phi_d$, proportional to the deramp frequency (and hence range) relating to a given point target and a resulting range estimate error, R_e, given by

$$\Delta\phi_d = 2\pi f_d\Delta t = \frac{4\pi BR\sqrt{\varepsilon_r}\Delta t}{cT} \quad \text{and}$$
$$R_e = \frac{\lambda\Delta\phi_d}{4\pi} = \frac{BR\Delta t}{f_cT} \tag{19}$$

For the present system, assuming a maximum range of 2 km and a desired range measurement accuracy of ±1 mm, a maximum timing error of ±0.75 μs and a maximum phase error of ±1.3° can be tolerated. This indicates that a quite stringent phase stability is required of the components in the RF chain, although the effect of temperature change on range indication may be readily calibrated, which is standard practice in many such measurements made by the British Antarctic Survey. The effects of a known timing error, Δt, can be cancelled by adding a further term to the reference array as follows

$$\text{ref} = \exp\left(-j(\omega_c\tau - K\tau^2/2) - 2\pi f_d\Delta t\right)$$
$$= \exp\left(-j(n\omega_c/Bp - n^2K/2B^2p^2) - 2\pi n\Delta t/Tp\right) \tag{20}$$

An out-of-band sinusoidal signal can be added to the radar output in order to aid synchronisation and obviate the need for hardware synchronisation of the chirp and ADC. It is important that the phase delay through the ADC is consistent over time to within a fraction of the tolerable timing error, 0.75 μs in this case. Linear phase anti-aliasing filtering would thus be preferable. In addition, the range estimate is directly proportional to the master clock frequency and so, for instance, a 1 ppm change in master clock frequency will give a 1 mm range estimate error at 1 km range. The prototype system therefore makes use of a high-performance 10 MHz HTFL/6E Stratum 3 TCXO source, with excellent long-term stability and temperature stability. The processing steps are summarised in Fig. 6.

On a practical note, the velocity of propagation in ice is sensitive to temperature, around 2.3×10^4 m/s/C, suggesting that a temperature change of 0.1 C will cause a measurement change of 5 mm over a 360 m path. Fortunately, ice that is deeper than 20 m or so is very stable thermally, as it is insulated by the snow and ice above, with annual temperature variations of a tiny fraction of a degree C. So the daily variation in mean ice temperature over the path from an internal layer to the basal layer is extremely small and its impact on the measurement in relation to the likely several mm/day melt rate is entirely insignificant. Spectral leakage is readily managed by zero-meaning the time-domain data to remove the DC component and using appropriate windowing – Blackman windowing being particularly effective.
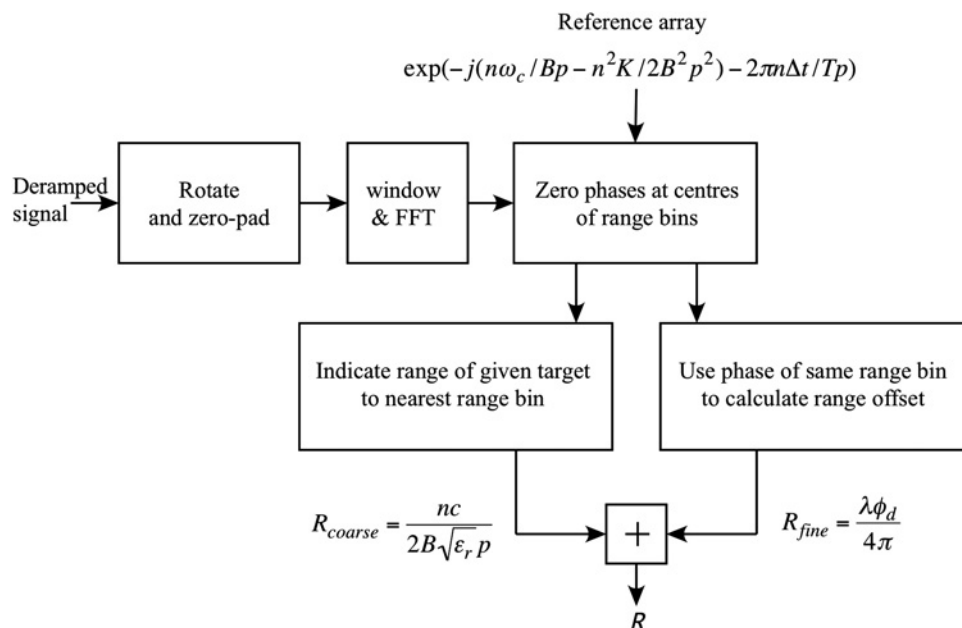

Fig. 6 *Summary of the phase-sensitive FMCW range processing steps*

4   Prototype system and results

The prototype radar system is pictured in Fig. 7. It is based on an elaboration of Fig. 1, including additional front-end filtering and digital clock generation and synchronisation. The system makes use of an Analog Devices AD9910 DDS synthesiser, generating a 200–400 MHz chirp signal with a 1 GHz clock. A pair of Mini-Circuits ZX76-31-PP+ digital step attenuators are employed to sequentially switch the receiver RF gain between values of 4, 16, 28 and 40 dB, on successive chirps, in order to provide a range of receiver gain settings to allow good performance with both near and far scatterers. A second-order high-pass filter is
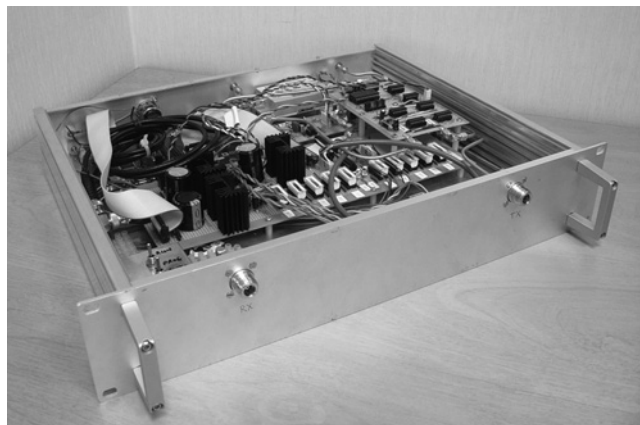

Fig. 7   *Photo of the prototype radar system*

incorporated, with a gain of 0 dB at frequencies below 50 Hz, rising to a peak of 80 dB at 5 kHz, in accordance with the predicted echo power levels indicated in Fig. 3. The instrument consumes 750 mA at 6 V when operating and 0.24 mA in standby, thus fulfilling the low-power consumption requirement (in relation to the predecessor 'pRES' system that consumed hundreds of Watts in operation and required a petrol generator). In addition, the much reduced noise figure allows much faster signal capture, further reducing the energy consumption.

A system model has been carefully constructed, based on the parameters listed in Table 1, in particular to assess phase-sensitive FMCW performance at low signal levels. Monte Carlo simulation, with 1000 trials, has been used to numerically estimate the RMS range measurement error as a function of signal strength for a test signal emulating a discrete target at 1800 m range in the presence of additive white Gaussian noise to simulate thermal noise. The processing includes peak detection in the vicinity of the known target, to establish the likely closest range bin. The modelled results, given in Fig. 8, show that the RMS range error increases from 1.3 mm for a −140 dBm receiver signal level to 14 mm for a −160 dBm signal level. The equivalent SNR (in the 1 Hz FFT bandwidth) over this range is 27.8–7.8 dB. These results are plotted alongside the simple analytic SNR expression of (8), and it is clear that there is very good agreement, even down to very low signal and SNR levels, significantly below the −154 dBm and 14 dB worst-case values expected at maximum range (2 km). It is observed that, at very low signal levels, occasional results are produced that are in error by approximately half a wavelength (284 mm). These are
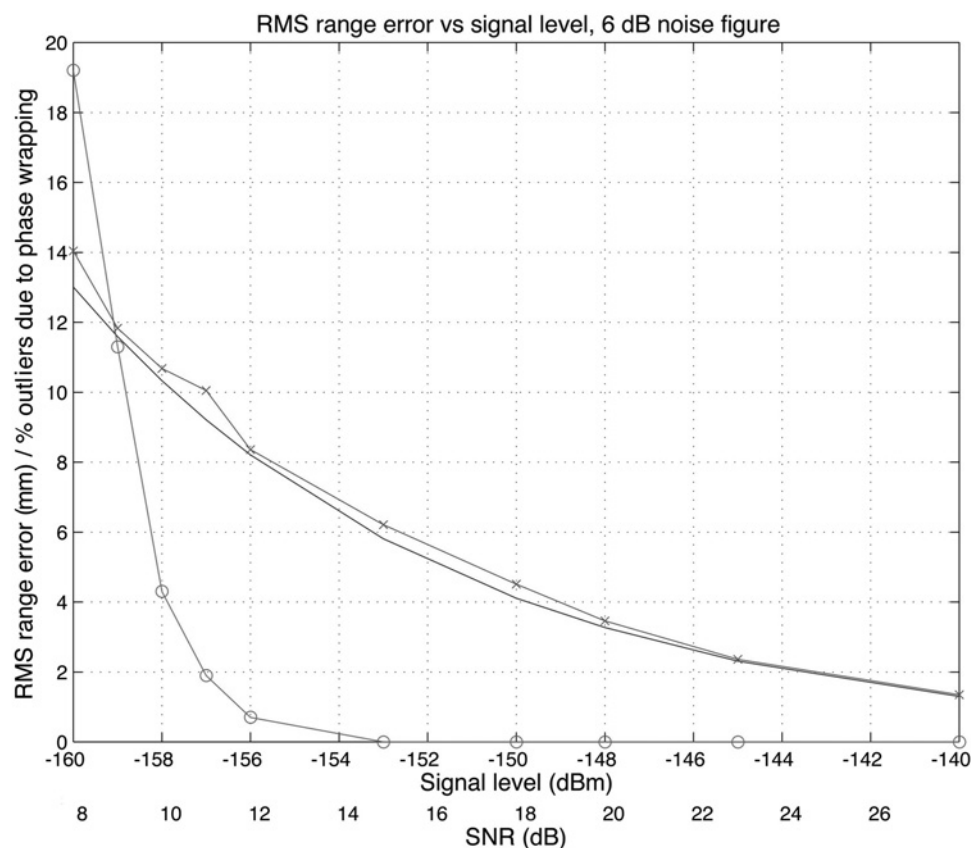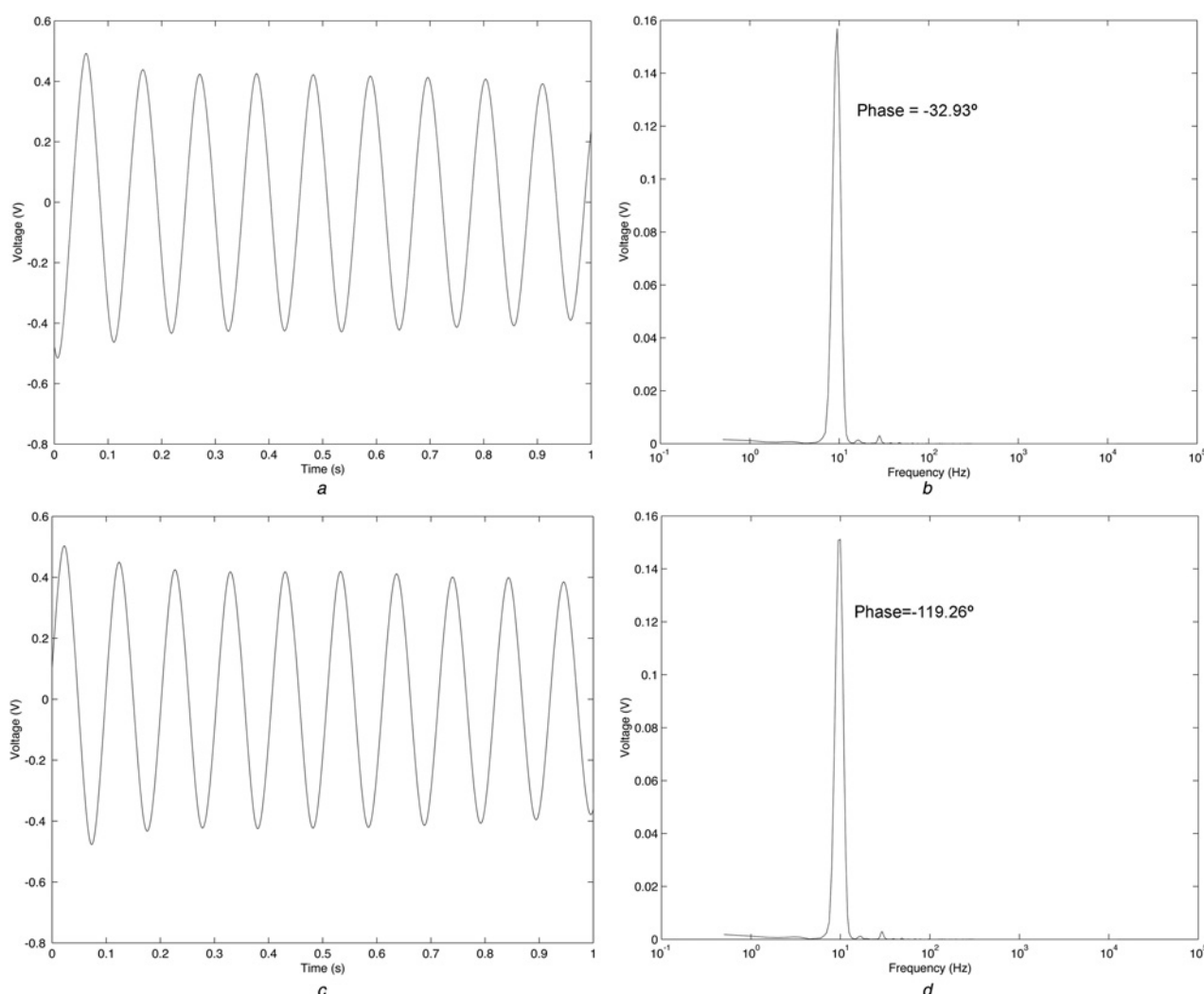

Fig. 8   *Modelled (×) and analytic (-) RMS range error against signal level and SNR*

Incidence of outlying results (of half-wavelength error) is also indicated (o)

Fig. 9 *Results of such a test using a cable of nominal length 10 m*

a, c Measured radar deramped time-domain signals

b, d Range-processed signals, during a Loop test with a nominal 10 m cable length [(a), (b)] and a 10 m + 14 in cable length [(c), (d)]

because of phase wrapping in the detected phase, as a result of noise, producing a near-360° error. The incidence of this effect is also plotted in Fig. 8 in which it is seen to be a very rare occurrence for signal levels above −154 dBm, while abruptly rising to some 19% incidence at a signal level of −160 dBm. Although these outlying results can be easily eliminated in the processing, this does suggest a distinct minimum signal threshold, of around −160 dBm or 7.8 dB SNR. This performance exceeds that required of the system.

A number of loop tests have been performed on the prototype radar to validate system performance. For these tests, the radar was operated with the transmit port connected to the receive port via a length of cable, attenuator and with zero front-end gain in the receive chain. Radar parameters were as indicated in Table 1, including a pad factor of 2 and an ADC sampling rate of 25 ksamples/s. A Blackman window is used, prior to FFT processing. The results of such a test using a cable of nominal length 10 m are shown in Fig. 9a (time-domain) and Fig. 9b (frequency domain). A dielectric constant of 2.1 is assumed for the cable and associated connectors, with a corresponding radar range resolution of 518 mm or 1.04 m round-trip path resolution. Classic radar range processing

would thus indicate cable length to some 1 m resolution in this instance. The target appears in the 9.5 Hz range bin, equating to a standard, coarse range estimate of 4.9167 m. The indicated phase [after normalisation as indicated in (17)] is −32.93° giving a fine range estimate of −31.6 mm

Fig. 10 *Instrument deployment at the Larsen-C ice shelf, Antarctica*
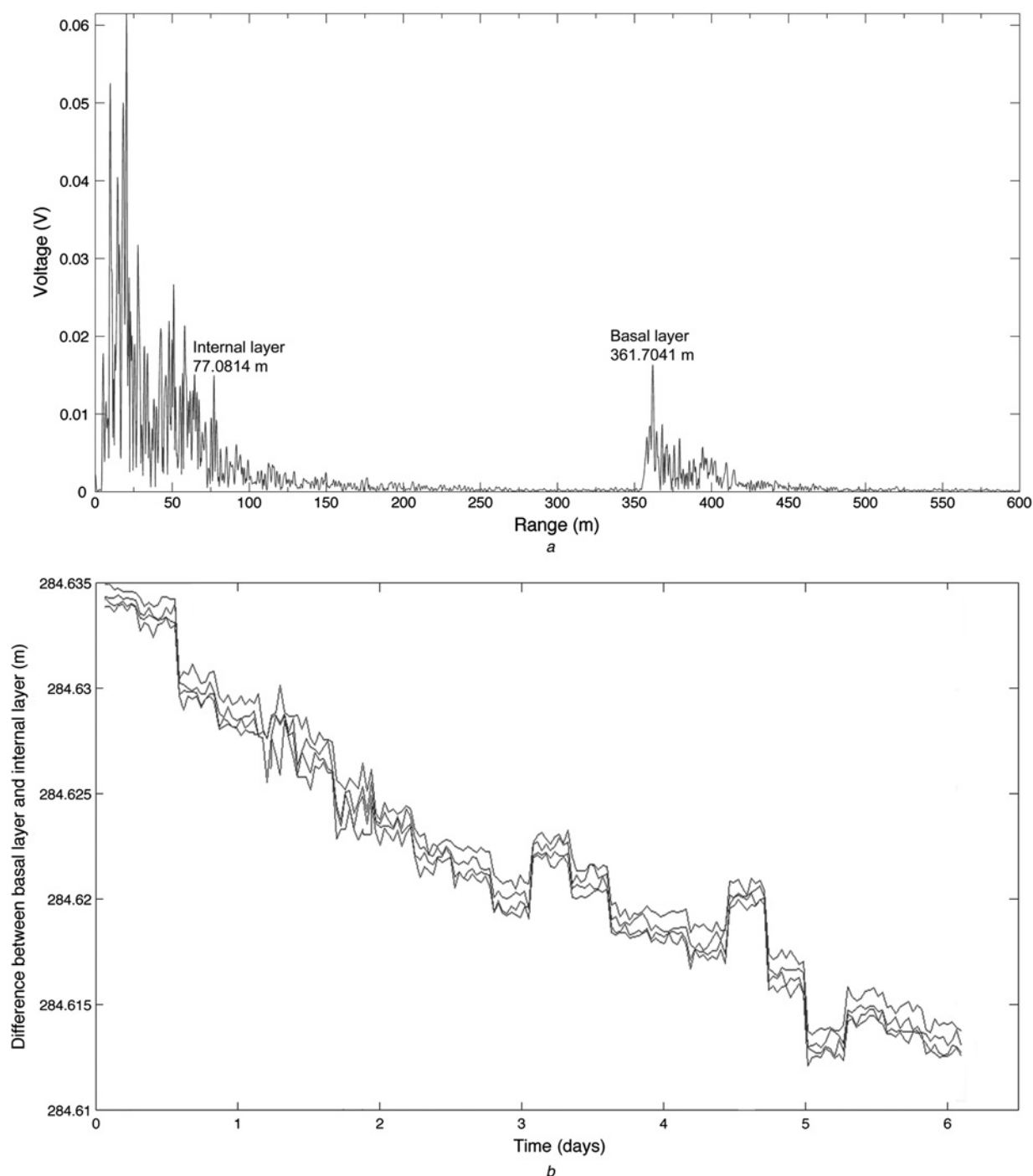
Fig. 11 *Measured results taken from the Larsen-C ice shelf, Antarctica showing*
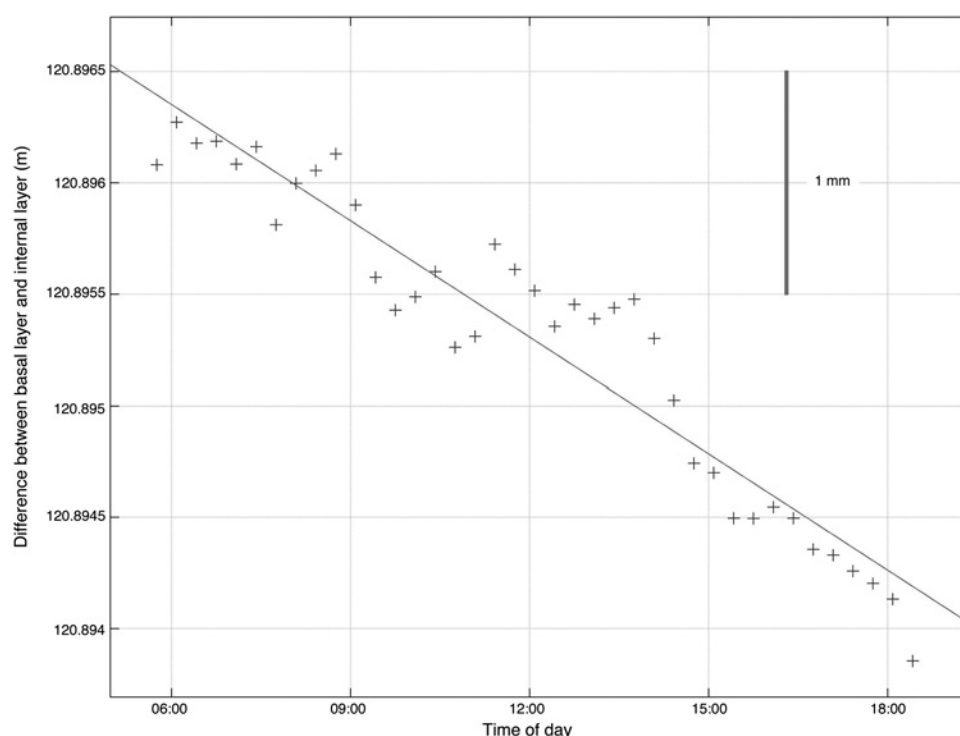
a Range profile
b Time series plot of the difference between basal layer and (77 m) internal layer depth, indicating a 3.5 mm/day thinning rate

and a resultant range, using phase-sensitive FMCW processing, of 4.8851 m, corresponding to a round-trip path and cable length estimate of 9.7702 m. The same cable was then extended by 35.56 cm using a length of additional cable and the measurement repeated. The results, in Figs. 9*c* and *d* show a notable shift in phase, but a small shift in frequency. The target peak now occurs in the 10 Hz range bin, equating to a standard, coarse range estimate of 5.1755 m. The indicated phase (after normalisation) is −119.26° giving a fine range estimate of −114.3 mm and a resultant range, using phase-sensitive FMCW processing, of 5.0612 m, corresponding to a round-trip path and cable length estimate of 10.1224 m. The additional path length is

thus measured as 35.22 cm, showing close agreement to the known additional cable length.

The instrument has been deployed at various locations in Antarctica, as pictured in Fig. 10 at the Larsen-C ice shelf. A series of range profile measurements has been obtained at Larsen-C, one of which is shown in Fig. 11*a*. This range profile clearly shows the basal layer at a depth of ~362 m and also a set of returns at closer range, from ~10 to 80 m. The largest return, at around 20 m, is because of direct transmit–receive coupling, but many of the returns from more shallow depths are reflections from internal layers. These layers are very stable and can be used as a reference to monitor the melt rate of the basal layer. An internal layer

Fig. 12 *Measured results taken from the Ross ice shelf, Antarctica, showing a time series plot of the difference between basal layer and (120 m) internal layer depth, indicating a 4.1 mm/day thinning rate*

at around 77 m has been selected for this purpose. The signal-to-clutter-and-noise ratio is very high and, indeed, at the basal layer the system noise is some 20 dB below clutter, indicating excellent radar sensitivity. Phase-sensitive FMCW processing has been used to measure the depth of the internal and basal layers to 0.1 mm precision, as indicated in Fig. 11*a* A 6-day time series of the differential measurement between the 77 m internal layer and the basal layer, is shown in Fig. 11*b*, where it should be appreciated that the extent of the *y*-axis is just 25 mm. Four results are presented for four different radar receiver gain settings, the radar cycling through these automatically in order to ensure sufficient dynamic range. Although there are some fluctuations in the results, there is a clear thinning trend, at a mean rate of 3.5 mm/day over this period. A further result obtained at the Ross ice shelf is shown in Fig 12, indicating the ice shelf thickness variation over a 12 h period. A straight line fit suggests a 4.1 mm/day thinning rate in this instance with the points scattered around this line with an RMS variation of ~0.2 mm, thus demonstrating the sub-mm precision of the instrument.

The standard technique for making these measurements, in view of the horizontal ice flow, is to allow the radar to move with the ice (rather than being at the same absolute location), thus taking the same ice column and section of base with it. Corr *et al.* [1] explains the procedure for doing this, by the use of surface markers around the radar site to provide a direct indication of the horizontal flow. The thinning rate results obtained with our instrument, of 3.5 and 4.1 mm/day from the Larsen-C and Ross ice shelves, respectively, compare very well with results for the same sites based on oceanographic and other indirect methods, of 3.0–4.1 mm/day at Larsen-C (Nicholls *et al.* [14]) and 4.2 mm/day at Ross (Stewart and Williams [15]), thus validating the accuracy of the instrument and the integrity of the results.

5 Conclusions

This paper has described a radar system designed for high-precision monitoring of the changing thickness of an Antarctic ice shelf. Such a radar is intended as an advance on a step-frequency radar that has been pioneered by the British Antarctic Survey to offer improved sensitivity and hence reduced integration time, reduced power consumption and the capability of year-round unmanned operation. A phase-sensitive FMCW architecture has been developed to fulfil this requirement.

Link budget modelling has been presented, indicating that performance to 3 mm RMS precision at 1.8 km is possible with modest transmit power (0.1 W) and with an integration time of 1 s. A detailed analysis of phase-sensitive FMCW radar operation has led to the development of innovative processing to achieve high-precision, unambiguous imaging of discrete targets, including data rotation, zero-padding phase normalisation of the range-processed radar signal for convenient calculation of the precise range. Timing synchronisation has been found to be critical for measurement repeatability, in which it is shown that 0.75 μs tolerance is required for 1 mm precision in this application.

Modelled results have been used to assess RMS range error performance at low signal levels, demonstrating very close agreement to a simple analytic result, which proves to be reliable to SNRs of around 8 dB. A prototype radar system has been developed and a number of loop tests performed, validating performance and demonstrating mm range measurement precision. Further results are presented from the Larsen-C and Ross ice shelves in Antarctica again demonstrating mm-precision performance and indicating thinning rates of 3.5 and 4.1 mm/day, respectively, which compare closely to other published results obtained using different methods, thus validating our measurements. The results and techniques presented in this paper are, of course,

applicable to phase-sensitive FMCW radar, in general, and it is hoped that they will be of value to others working on these systems.

6 References

1 Corr, H.F.J., Jenkins, A., Nicholls, K.W., Doake, C.S.M.: 'Precise measurement of changes in ice-shelf thickness by phase-sensitive radar to determine basal melt rates', *Geophys. Res. Lett.*, 2002, **29**, (8), p. 1232

2 Jenkins, A., Corr, H.F.J., Nicholls, K.W., Stwart, C.L., Doake, C.S.M.: 'Interactions between ice and ocean observed with phase-sensitive radar near an Antarctic ice-shelf grounding line', *J. Glaciol.*, 2006, **52**, (178), pp. 325–346

3 Cardenas, C.A., Jenett, M., Schunemann, K., Winkelmann, J.: 'Sub-ice topography in Patriot Hills, West Antarctica: first results of a newly developed high-resolution FM-CW radar system', *J. Glaciol.*, 2009, **55**, pp. 162–166

4 Griggs, J.A., Bamber, J.L.: 'Antarctic ice shelf thickness from satellite radar altimetry', *J. Glaciol.*, 2011, **57**, (203), pp. 485–498

5 Laxon, S.: 'Sea ice extent mapping using the ERS-1 radar altimeter', *EARSeL Adv. Remote Sens.*, 1994, **3**, (2 – X11), pp. 112–116

6 Skolnik, M.I.: 'Radar handbook' (McGraw-Hill, 2008, 3rd edn.)

7 Jol, H.M.: 'Ground penetrating radar: theory and applications' (Elsevier, 2009)

8 Bragg, W.L.: 'The diffraction of short electromagnetic waves by a crystal'. Proc. Cambridge Philosophical Society, 1913, vol. 17, pp. 43–57

9 Brennan, P.V.: 'Phase-locked loops, principles and practice' (Macmillan, 1996), ISBN 0 333-65571-0, McGraw-Hill ISBN 0-07-007568-9

10 Robins, W.P.: 'Phase noise in signal sources (theory and applications)' (Peter Peregrinus I.E.E. Telecommunications Series, 1982)

11 Ayhan, S., Pahl, P., Kayser, T., Pauli, M., Zwick, T.: 'Frequency estimation algorithm for an extended FMCW radar system with additional phase evaluation'. Proc. Sixth German Microwave Conf., Darmstadt, Germany, March 2011

12 Woods, G.S., Maskell, D.L., Mahoney, M.V.: 'A high accuracy microwave ranging system for industrial applications', *IEEE Trans. Instrum. Meas.*, 1993, **42**, pp. 812–816

13 Qi, G.: 'High accuracy range estimation of FMCW level radar based on the phase of the zero-padded FFT'. Int. Conf. Signal Processing, August 2004, vol. 3, pp. 2078–2081

14 Nicholls, K., Makinson, K., Venables, E.: 'Ocean circulation beneath Larsen C Ice Shelf, Antarctica from in situ observations', *Geophys. Res. Lett.*, 2012, **39**, (19), p. L19608

15 Stewart, C., Williams, M.: 'Melting and ocean circulation at the front of the Ross ice shelf'. Strategic Science in Antarctica Conf., Hobart, Tasmania, June 2013